Graphical Abstract

Optimising Point Source Irradiation of a Capsule for Maximum Uniformity

Oliver Breach, Peter Hatfield, Steven Rose

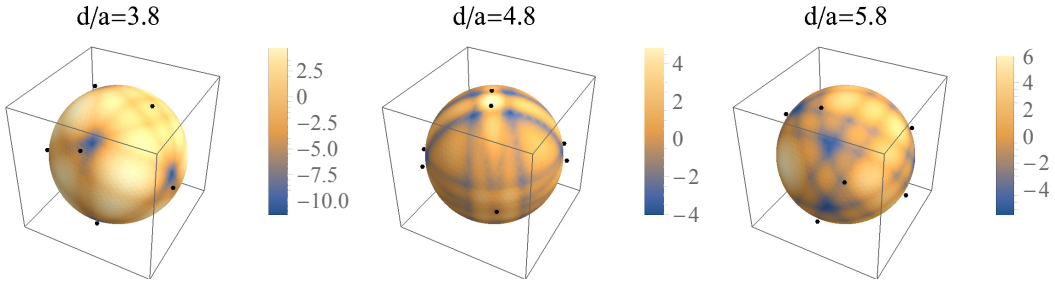

Highlights

Optimising Point Source Irradiation of a Capsule for Maximum Uniformity

Oliver Breach, Peter Hatfield, Steven Rose

- Use of a mixed analytic and algorithmic approach to the optimisation of illumination symmetry for ICF
- The approach taken found novel geometric arrangements of X-ray sources that minimised nonuniformity which were not anticipated
- These novel arrangements were interpreted and explained through a modal analysis

Optimising Point Source Irradiation of a Capsule for Maximum Uniformity

Oliver Breach[a], Peter Hatfield[b], Steven Rose[c]

[a]*Department of Physics, University of Cambridge, J. J. Thomson Ave, Cambridge, CB3 0HE, UK*
[b]*Department of Astrophysics, Oxford University, Keble Rd, Oxford, OX1 3RH, UK*
[c]*Plasma Physics Group, Imperial College London, South Kensington Campus, London, SW7 2AZ, UK*

Abstract

Inertial Confinement Fusion involves the implosion of a spherical capsule containing thermonuclear fuel. The implosion is driven by irradiating the outside of the capsule by X-rays or by optical laser irradiation, where in each case the highest uniformity of irradiation is sought. In this paper we consider the theoretical problem of irradiation of a capsule by point sources of X-rays, and configurations which maximize uniformity are sought. By studying the root-mean-square deviation in terms of different order harmonic modes, we rationalise the dependence of uniformity on distance d of the point sources from the centre of a capsule. After investigating simple configurations based on the Platonic solids, we use a global optimisation algorithm (basin-hopping) to seek better arrangements. The optimum configurations are found to depend strongly on d; at certain values which minimise nonuniformity, these involve grouping of sources on the vertices of octahedra or icosahedra, which we explain using a modal decomposition. The effect of uncertainties in both position and intensity is studied, and lastly we investigate the illumination of a capsule whose radius is changing with time.

Keywords: ICF, indirect drive, machine learning, optimisation

1. Introduction

The field of Inertial Confinement Fusion (ICF) started in the open literature in 1972 with Nuckolls et al. [1], who considered the use of a spherical implosion to create a plasma of DT fuel that would undergo thermonuclear

reactions. Nuckolls et al. considered an implosion driven by directly illuminating the spherical capsule by high-power optical laser radiation. These original calculations suggested that energy gain could be obtained using less than 10 kJ of laser energy. Over the intervening years there has been huge progress in ICF research, both experimentally in laser and target physics and theoretically in modelling; the most recent results have shown a gain of around 0.7, in which the laser (the National Ignition Facility, NIF, in the USA) delivers around 2 MJ of energy to the target [2]. Work at the NIF still employs a spherical implosion of the DT fuel but the laser does not directly heat the capsule — rather the laser heats a gold or gold-uranium cavity (hohlraum) that produces an X-ray bath, which irradiates the capsule and drives the implosion (so-called indirect-drive). Direct laser irradiation of a capsule is still being pursued (notably at the Laboratory for Laser Energetics in Rochester, USA) and because of the inefficiencies in the indirect-drive method, direct-drive is a serious contender for a future scheme that can achieve high-gain.

The irradiation uniformity of the spherical capsule during its implosion is of critical importance to the implosion's performance, whether using indirect- or direct-drive, and has been extensively studied both theoretically and experimentally [3]. Motivated by this, in this paper we consider a theoretical problem of the irradiation of a spherical capsule by point sources of X-rays placed at some distance from the capsule. We aim to understand the interplay between their geometric arrangement and irradiation uniformity. We assume that the sources radiate X-rays in a spherically symmetric fashion, such as would occur from laser irradiation of solid point targets (as have been used extensively in X-ray backlighting experiments for many years [4]) or of small spherical capsules which would produce a short-lived X-ray flash from their implosion. Our work on this method of irradiation stems from our interest in investigating the use of these point sources to develop an X-ray drive for the central spherical capsule that has a faster rise-time than can be achieved with a conventional hohlraum. Such fast rise-times are of interest in driving new capsule designs, including those employing 'shock ignition' [5]. Although shock ignition has been seriously considered for direct-drive, the need for a fast rising X-ray drive has precluded extensive study in the indirect-drive mode; we note, however, that progress towards indirect drive shock-ignition is being made [6, 7].

We first investigate configurations based on the sources arranged at the vertices of the Platonic solids, which provide a good benchmark for achiev-

able uniformities. Despite the problem seeming equivalent to the well-known mathematical problem of the 'Spherical Code' [8] we show that this is not the case; using the formalism first presented by Skupsky and Lee [9], we explain this through the elimination of certain modes. Machine-learning [10] is then employed to discover improved configurations using the basin-hopping method [11], a global-optimisation technique developed for atomic-cluster energy minimization. This allows us to find arrangements that improve significantly on the Platonic solids. We then extend the formalism to account for the variation in the size of the capsule over time, and find that the new optimised configurations are different to the stationary case. An investigation of various arrangements' stability to uncertainties in position and intensity is also conducted.

2. Formalism

First consider a single point source of strength S at a distance d from the centre of the capsule of radius a. The point source radiates in a spherically symmetric manner with intensity $S/4\pi r^2$ at a distance r from the source. At a polar angle of θ relative to the point source, the power delivered per unit surface area on the capsule is given by

$$I(\theta) = \frac{S}{4\pi} \frac{d\cos\theta - a}{(d^2 + a^2 - 2ad\cos\theta)^{3/2}},\ 0 \leq \theta \leq \arccos(a/d). \tag{1}$$

For a collection of point sources, such as in Fig. 1, the intensity is the linear superposition of intensities due to the individual sources; this is a good approximation for X-ray drive.

To measure the nonuniformity we use the normalised standard deviation σ_{rms}, defined by

$$\sigma_{rms}^2 = \frac{1}{\bar{I_T}^2} \left(\frac{1}{4\pi} \int \left(I(\vec{r}) - \bar{I_T} \right)^2 d\vec{r} \right), \tag{2}$$

where $\bar{I_T}$ is the mean intensity over the sphere, and the integral is over the entire capsule surface. An alternative metric is the maximum absolute deviation from the mean. We found that these two metrics are in qualitative agreement in that the configurations that are particularly nonuniform in one metric are found to be nonuniform in the other.

Following Skupsky and Lee [9], this expression can be simplified in the case where all point sources are at the same distance d. Suppose the kth

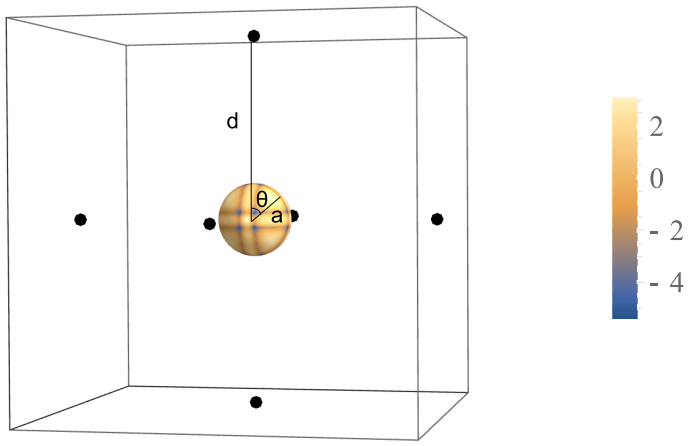

Figure 1: Example configuration with 6 sources in the octahedral arrangement, with $d/a = 5$. The black points represent the sources, and the capsule is the coloured sphere - the colours represent the percentage deviation from the mean intensity according to the scale. θ is the angle from a given source to an arbitrary point on the capsule. The grey surrounding cube provides perspective.

source is in the direction of the unit vector $\vec{\Omega}_k$. Then because the intensity is axisymmetric, we can expand the intensity on the capsule of a single source in Legendre polynomials:

$$I_k(\theta) = \bar{I}_k \left(1 + \sum_{l=1}^{\infty} a_l P_l \left(\cos\theta \right) \right). \tag{3}$$

Here $\bar{I}_k$ is the mean intensity over the capsule due to the kth source, and θ is the angle between the unit vector $\vec{\Omega}_k$ and the point of interest. Subsequently σ_{rms} may be decomposed into the contributions from individual modes:

$$\sigma_{rms}^2 = \sum_{l=1}^{\infty} \sigma_l^2 = \sum_{l=1}^{\infty} \frac{a_l^2}{2l+1} G_l^2 \tag{4}$$

where

$$G_l^2 = \sum_{j=1}^{N} \sum_{k=1}^{N} P_l \left(\vec{\Omega}_j \cdot \vec{\Omega}_k \right) \frac{\bar{I}_j \bar{I}_k}{\bar{I}_T{}^2}. \tag{5}$$

The nonuniformity has now been separated into terms corresponding to the profile of a single source a_l (defined through Eq. (3)), and geometric factors related to the relative positioning of the sources G_l. We will make extensive use of this in the following sections.

3. High Symmetry Configurations and Dependence on d

In this section we explore configurations constructed by placing sources at the vertices of Platonic solids, and evaluate their uniformity. In Table 1 we record the maximum deviation from the mean and σ_{rms} for the five Platonic solids — tetrahedron, octahedron, cube, icosahedron, and dodecahedron. We have also included the square anti-prism (8 sources), and 'Spherical Code 20' (20 sources), which are the solutions to the 'Spherical Code' problem – how can n points be distributed on a unit sphere such that they maximize the minimum distance between any pair of points – that are not Platonic solids [8]. For 8 sources, the cube outperforms the square anti-prism, so we deduce that maximising uniformity is not equivalent to the 'Spherical Code'.

Table 1: Nonuniformity for platonic solids and other high symmetry shapes. Here, d/a is the ratio of distance of sources to radius of capsule which minimises the nonuniformity, which is specified first in terms of the maximum percentage difference from the mean intensity, and secondly as the standard deviation of intensity σ_{rms}.

Shape	d/a	Max Deviation / %	σ_{rms} / %
Tetrahedron (4)	∞	18.3	7.52
Octahedron (6)	4.82	5.02	1.63
Cube (8)	4.95	4.8	1.44
Square Anti-prism (8)	∞	14	7.53
Icosahedron (12)	2.55	1.83	0.68
Dodecahedron (20)	2.54	1.39	0.527
Spherical Code 20 (20)	2.54	1.39	0.526

The nonuniformity is strongly dependent on the distance of the sources from the capsule. In Table 1 we have included the value of d/a which optimises the uniformity. To understand this, Fig. 2 plots σ_{rms} against d/a for the tetrahedron, octahedron, and icosahedron. The existence of minima for the octahedron and icosahedron can be understood intuitively through a consideration of different regimes. When the sources are very close to the capsule, the intensity will be a maximum just below the sources. However, at larger d/a, the maxima will occur where we have contributions from the most point sources. In between, there will be a case when the intensity is most 'spread out', increasing uniformity. This is demonstrated for the octahedron in Fig. 3. For the tetrahedron, there is another competing factor

which washes out the minimum — the transition between the two regimes mentioned above occurs at d/a close to 1, when there is still a rapid decrease in nonuniformity due to the spreading out of intensity from single point sources. Finally, we note that the nonuniformity tends to a finite limit as $d/a \to \infty$, which for n sources is given by

$$\sigma^2_{rms}(d/a \to \infty) = \frac{1}{n^2} \int \left(4 \sum_i (\cos\theta_i \; H(\pi/2 - |\theta_i|)) - n \right)^2 d\vec{r}, \qquad (6)$$

where $H(y)$ is the step function - $H(y > 0) = 1$ and $H(y < 0) = 0$ - so that the $\cos\theta_i$ terms only apply for $\theta_i \leq \arccos(a/d) \to \pi/2$.

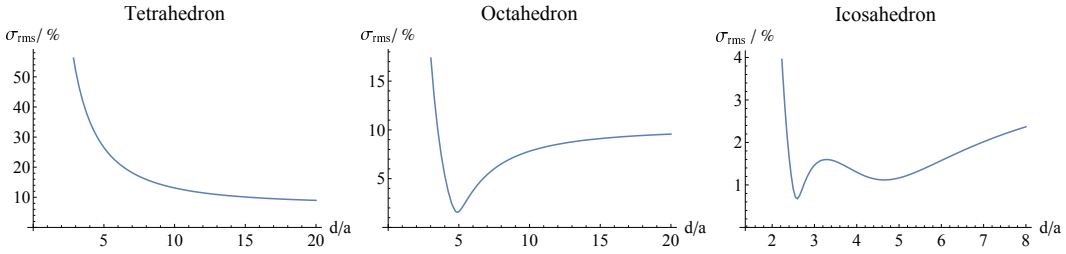

Figure 2: σ_{rms} against d/a for three different arrangements, demonstrating how uniformity depends on distance of sources from the capsule. Note the minima for the octahedron and icosahedron.

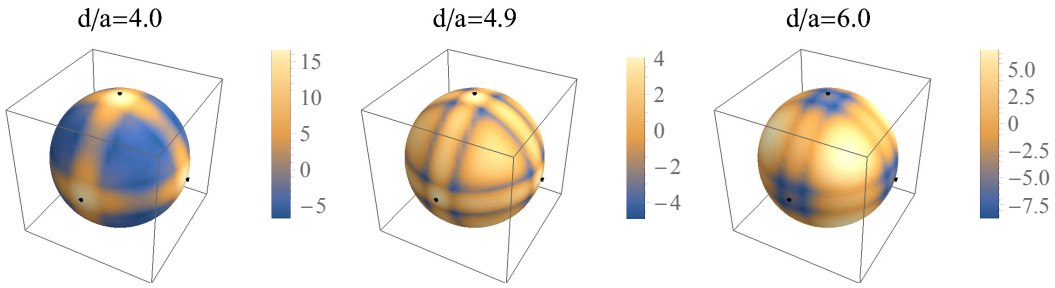

Figure 3: Intensity distribution on the surface of the capsule for the octahedral arrangement for varying values of d/a. Uniformity is maximised for $d/a = 4.9$, in the intermediate region between the two regimes demonstrated to either side. The scale shows the percentage deviation from the mean, and the blue points represent the angular positions of the sources — distances are not to scale.

4. Relation to Formalism

The existence of the minima shown in Fig. 2 can be understood in relation to the formalism described in Section 2. First, consider the G_l^2 factors plotted in Fig. 4. For the octahedron and icosahedron, all odd modes vanish; this is shown to be true whenever we have pairs of sources symmetric with respect to the centre of the capsule in Ref. [9]. Despite the G_l^2 terms decreasing only slowly with l, the typical scale of the a_l terms decreases rapidly — hence the lowest non-zero G_l term dominates the nonuniformity. For the tetrahedron, this is $l = 3$; the dominant term in the nonuniformity is thus $\sigma_{rms}^2 \approx \frac{1}{7}a_3^2 G_3^2$. Looking at how a_3 depends on d/a in Fig. 5, we can then deduce that σ_{rms}^2 monotonically decreases, agreeing with Fig. 2. For the octahedron however, the dominant term is $l = 4$, which has a minimum (becoming zero) at $d/a = 4.84$ — this is very close to the position which minimises the nonuniformity in Table 1. Finally, for the icosahedron the two minima in Fig. 2 correspond to the two zeros in the l=6 mode in Fig. 5.

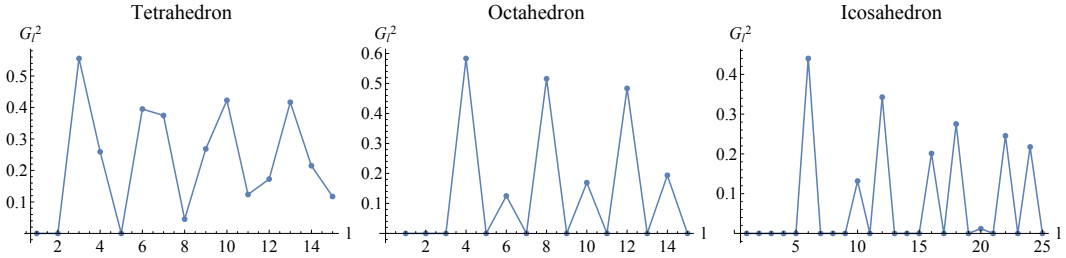

Figure 4: G_l^2 against mode number l for the tetrahedron, octahedron, and icosahedron. Plots of this form (G_l^2 against mode number) appear in Ref. [3].

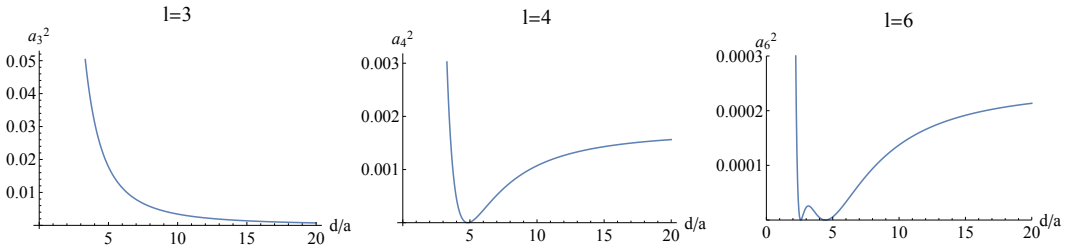

Figure 5: a_l^2 against d/a for l=3,4,6 — the dominant modes for tetrahedron, octahedron, and icosahedron respectively. Comparing to Fig. 2 demonstrates that these are indeed the dominant modes.

5. Optimisation

In this section we seek improvements on the 'symmetric' configurations described in the previous sections. We will now allow not only positions but also intensities to vary. All sources will be kept at the same distance, but we repeat the optimisation for a range of d/a values; indeed, it will turn out that $d/a = 4.84$ and 2.59 are optimal, since these values eliminate the $l = 4$ and 6 modes respectively.

5.1. Optimisation Algorithms

Global optimisation is a well researched topic with a wealth of available methods [12, 13]. Algorithms typically fall into two categories — those which require derivatives, and those which do not. If we seek to minimize the maximum deviation from the mean, derivatives are not easily available and we must use derivative-free optimisation procedures, such as genetic algorithms [14]. However, writing σ^2_{rms} as in Eq. (4), derivatives may be calculated straightforwardly, opening up a wider range of strategies.

Due to the high numbers of degrees of freedom, with many local minima, this problem is very similar to that of finding the lowest energy structures of Lennard-Jones atom clusters. Accordingly, we use a technique called 'basin-hopping' [11], developed specifically for these atom clusters, which combines local optimisation with random perturbations, accepting perturbations according to a Metropolis criterion. In this work we used the implementation developed by SciPy [15].

5.2. Derivatives

For the local minimisation the L-BFGS-B algorithm[16] was used to cope with the high dimensionality of the problem. At fixed d/a, the a_l terms are constant, and the required derivatives are those of G^2_l given by:

$$\frac{\partial G^2_l}{\partial \theta_i} = 2 \sum_k P'_l \left(\vec{\Omega}_i \cdot \vec{\Omega}_k \right) \frac{\partial \vec{\Omega}_i}{\partial \theta_i} \cdot \vec{\Omega}_k \frac{\bar{I}_i \bar{I}_k}{\bar{I_T}^2} \tag{7}$$

$$\frac{\partial G^2_l}{\partial \phi_i} = 2 \sum_k P'_l \left(\vec{\Omega}_i \cdot \vec{\Omega}_k \right) \frac{\partial \vec{\Omega}_i}{\partial \phi_i} \cdot \vec{\Omega}_k \frac{\bar{I}_i \bar{I}_k}{\bar{I_T}^2} \tag{8}$$

$$\frac{\partial G^2_l}{\partial \bar{I}_i} = \frac{2}{\bar{I_T}^2} \sum_k P_l \left(\vec{\Omega}_i \cdot \vec{\Omega}_k \right) \bar{I}_k - \frac{2}{\bar{I_T}^3} \sum_j \sum_k P_l \left(\vec{\Omega}_j \cdot \vec{\Omega}_k \right) \bar{I}_j \bar{I}_k \tag{9}$$

where

$$\vec{\Omega}_i = \begin{bmatrix} \sin\theta_i \cos\phi_i \\ \sin\theta_i \sin\phi_i \\ \cos\theta_i \end{bmatrix}. \tag{10}$$

We then have

$$\frac{\partial \sigma_{rms}^2}{\partial q} = \sum_{l=1}^{\infty} \frac{a_l^2}{2l+1} \frac{\partial G_l^2}{\partial q} \tag{11}$$

where q is either θ_i, ϕ_i, or $\bar{I}_i$ (which is directly proportional to the source strength S_i).

5.3. Results

For greater than 5 sources, the best uniformities were found near $d/a = 4.84$ and 2.59. The nonuniformity for each is plotted in Figs. 6 and 7; in all cases bar 6 sources, the results improve on those in Section 2. Studying the resulting configurations, with examples for $d/a = 4.84$ in Fig. 8, reveals the surprising fact that they do not necessarily spread points out as far as possible. Indeed, for more than 5 sources at $d/a = 4.84$, we observe clustering into an octahedral arrangement, with the resulting intensities of the sources adjusted such that the total intensity at each vertex is approximately the same. Similarly, for more than 12 sources at $d/a = 2.59$, sources cluster into an icosahedral arrangement. The difference of the solutions from those of the Spherical Code is clear, and the differences in uniformity are noticeable. For example, for 12 sources at $d/a = 4.84$ an icosahedron obtains $\sigma_{rms} = 1.13\%$, whereas octahedral 'pairing' (still with the same intensities) reaches $\sigma_{rms} = 0.96\%$.

The reason for this clustering comes down to considering the contributions of various modes. At $d/a = 4.84$, the single source profile factor a_l vanishes for $l = 4$ (Fig. 5). Correspondingly, it is beneficial to make the geometric factor G_4 large since this comes with no cost in uniformity, whilst decreasing the G_l terms for higher modes. This is exactly what the octahedron achieves, as demonstrated in Fig. 4. Similarly, $a_6 = 0$ for $d/a = 2.59$, so it is beneficial to adopt an icosahedral arrangement which ensures G_6 large whilst forcing $G_4 = 0$. The slight separation of the sources at each vertex simply reduces intensity directly below this vertex, spreading irradiation out more. Finally, for even numbers of sources we always have pairs of sources symmetric with respect to the centre of the capsule, which eliminates all odd modes.

With fewer than 6 and 12 sources at $d/a = 4.84$ and 2.59 respectively, this mode elimination by clustering is not possible. In this case, the geometric arrangements are the solutions to the Spherical Code, but the relative intensities of sources may differ. For example, at $d/a = 2.59$ with 7 sources, we find two at the 'poles' with the remaining 5 around the 'equator'. Those at the poles have intensity 18% larger.

The one exception to this rule is 10 sources, which does not resemble the Spherical Code at $d/a = 2.59$. In fact, 10 sources illustrates the important point that the best configuration depends on the value of d/a, going through 3 different configurations, all plotted in Fig. 9. Finally, we note that the clustering observed above survives for only a small range of d/a values. For example, for octahedral clustering this region is $4.71 - 5.00$. Away from these regions, we return to 'spread-out' solutions — in some cases these align with the spherical code. More generally, this dependence on d/a highlights how the best arrangement will depend on the exact method of irradiation of the capsules.

All results were confirmed independently via direct numerical integration of Eq 2.

5.4. Further Algorithm Improvements – Reducing Degrees of Freedom

Eliminating all odd modes will generally give a large increase in uniformity. Thus, in implementing the algorithm, we can fix sources to be symmetric, which halves our number of degrees of freedom. Furthermore, to 'fix' in place the configurations and reduce the rotational symmetry, we fixed one point source at $(\theta, \phi) = (0, 0)$, and fix another with $\phi = 0$, reducing the degrees of freedom further by 3. This allows more efficient searches for larger numbers of sources.

6. Imperfections

As well as having small σ_{rms}, the configurations must be stable to the small imperfections present in experimental setups. Whilst Murakami et al. [17] develop an analytical model to study imperfections, here we take a more basic approach. After specifying potential uncertainties in the angles and intensities, an ensemble of 5000 new configurations were generated as perturbations from the optimum. σ_{rms} was then calculated for each; in Fig. 10, the ensemble mean and standard deviation of σ_{rms} is presented for various numbers of sources. The standard deviation in angles was taken as 0.035 rad,

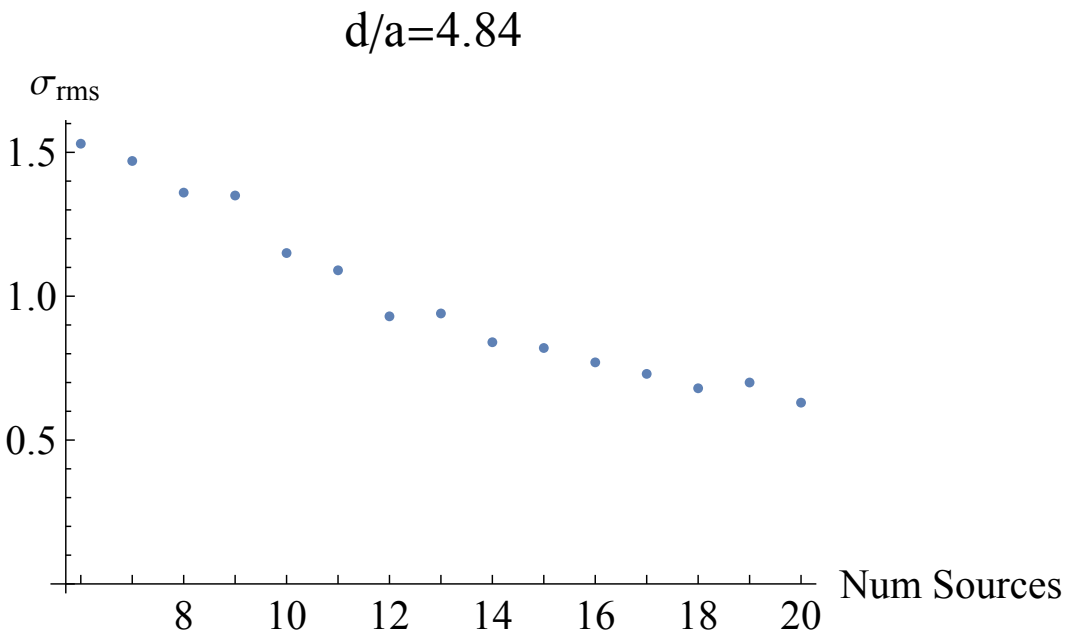

Figure 6: σ_{rms} against number of sources for configurations found by basin-hopping at $d/a = 4.84$. As with most optimisation problems, we cannot know for certain whether or not the global minimum has been found in each case.

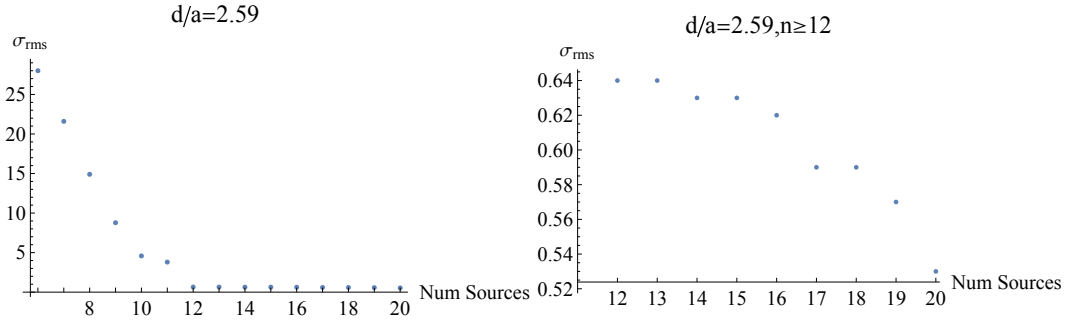

Figure 7: σ_{rms} against number of sources for configurations found by basin-hopping at $d/a = 2.59$. The right hand graph displays results for 12 or more sources only.

and that in the intensity as 2%. Comparing to Fig. 6 shows that the impact of these nonuniformities is large, typically by at least a factor of 2.

Due to the greater curvature around the minimum of the l=6 mode at $d/a = 2.59$ than the l=4 mode at $d/a = 4.84$ (Fig. 5), the impact of imperfections is even greater. However, at this smaller value of d/a a larger

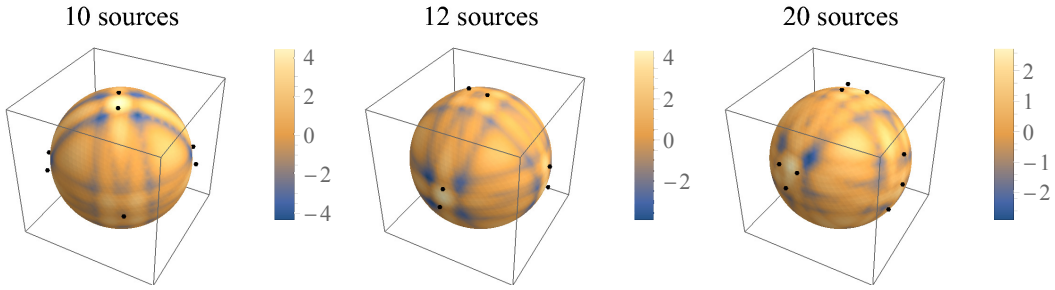

Figure 8: Intensity distributions on the surface of the capsule for 10, 12, and 20 sources in basin-hopping configurations, with $d/a = 4.84$.

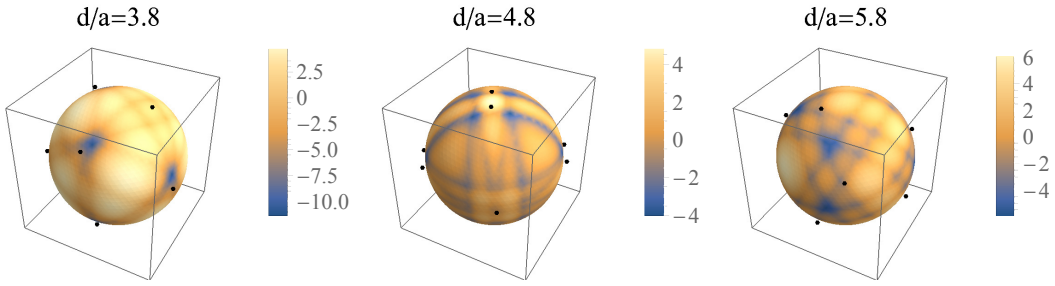

Figure 9: The optimal configuration for ten sources for a range of d/a values. The configuration is different in each case. For lower values of d/a we have two sources at the 'poles', and two 'rings' of 4 sources which are offset with respect to each other; those not at the poles have an intensity 1.23 times larger than the poles. At larger distances, we do now see the Spherical Code solution, with two rings of 5 sources.

proportion of energy irradiated by the point source reaches the capsule itself, leading to higher efficiency.

7. Change in Size of Capsule During Implosion

In an implosion, the radius of the capsule is changing as a function of time. Thus, to maintain uniformity over the whole time period, we should aim to minimize the standard deviation of the time averaged intensity. Fortunately, this is relatively simple to account for, since we are only required to change the a_l values to 'effective' values a'_l accounting for the time averaging. Denoting

$$\langle I(\vec{r})\rangle = \frac{1}{T}\int I(\vec{r},t)\,dt \tag{12}$$

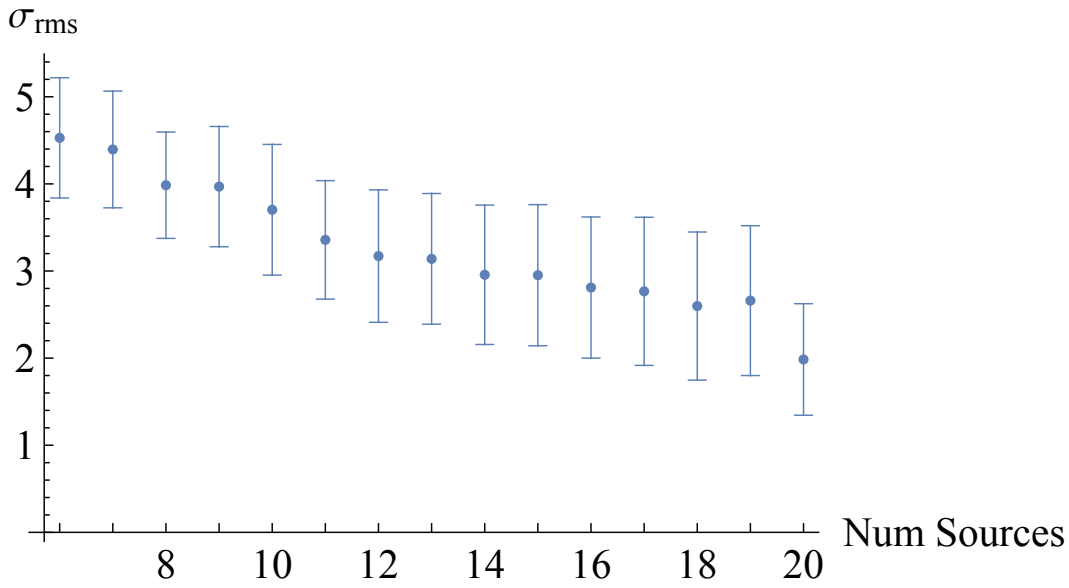

Figure 10: Mean σ_{rms} after perturbations from the optimum configurations at $d/a = 4.84$. Standard deviations in theta and phi are 0.035 rad, and in source strengths are 0.02% of the mean strength.

then writing

$$\langle I_k(\theta, t)\rangle = \left\langle \bar{I}_k \right\rangle \left(1 + \sum_{l=1}^{\infty} a'_l P_l\left(\cos\theta\right)\right), \tag{13}$$

we have

$$a'_l = \frac{1}{T}\frac{1}{\left\langle \bar{I}_k \right\rangle}\int \frac{2l+1}{2}\int I(\vec{r}, t) P_l(\cos\theta)\, d(\cos\theta)\, dt. \tag{14}$$

We used the data shown in Fig. 12, taken from Ref. [17], to calculate the a'_l values. Comparing Fig. 11 to Fig. 5, we see that the overall form of the curves is very similar, but the minima occur at different d/a values. For a'_4, the zero is at $d/a = 4.127$, whilst for a'_6 the first zero is at $d/a = 2.587$ and second at $d/a = 3.515$.

If we choose values of d/a corresponding to the zeros for the a'_4 or a'_6 terms, we recover the beneficial 'pairing' up in octahedral and icosahedral structures respectively, as in Subsection 5.3. This is for exactly the same reason as before - the maximum geometric term G_l is removed by the single source term a'_l being zero. Indeed, because of this qualitative similarity between the a_l and a'_l curves, the behaviour of the solutions is almost identical, but the

relevant values of d/a are different.

These calculations do not account for the fact that it is more important to minimize perturbations early in the implosion, since they have more time to grow. A potential solution is using a weighted time-average which gives greater weight to earlier times. Again, this would only modify the a_l terms required, and all previous techniques/analysis still apply.

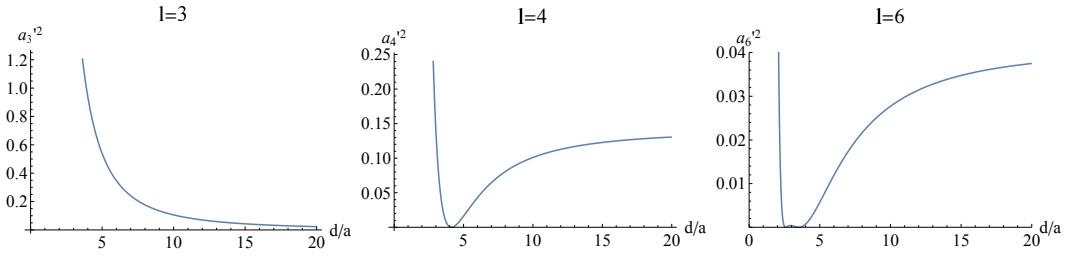

Figure 11: $a_l'^2$ against d/a for l=3,4,6. These coefficients take into account the time-averaging.

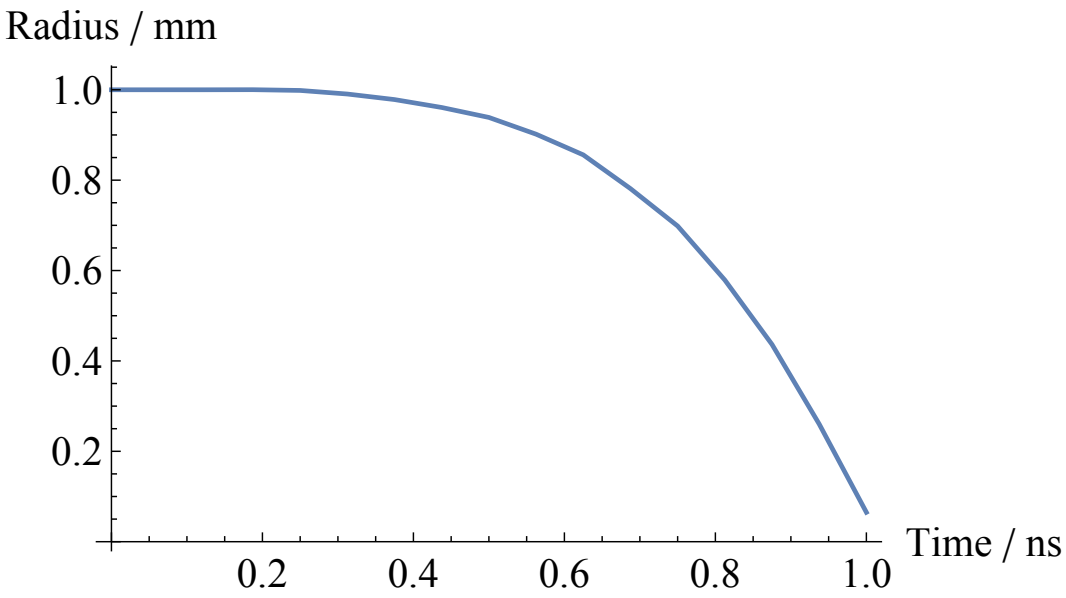

Figure 12: Radius of the capsule as a function of time during the implosion, from Ref. [18]

8. Conclusions and Further Ideas

The uniformity of irradiation of a capsule due to point sources was studied, and optimum configurations were sought. Based on initial 'high-symmetry' guesses of the Platonic solids and solutions to Spherical Codes, we found that the root-mean-square deviation was highly dependent on the distance of the sources from the capsule. Decomposing the nonuniformity into a sum of spherical harmonics, the existence of minima with respect to this distance was shown to be a result of the vanishing of certain modes.

Basin-hopping with local L-BFGS-B minimization was made possible by this mode decomposition, and then used to seek new configurations. The highest uniformities were found at two different distances, corresponding to the vanishing of the $l = 4$ and $l = 6$ modes. For the former, it was beneficial to group sources together around the vertices of an octahedron, whilst for the latter when there were greater than 12 sources, icosahedral arrangements were favourable. Studying the best configurations across a range of distances yielded two further insights. Firstly, that the best configuration often changed significantly at different distances — this demonstrates that configurations must be chosen with respect to the specific method of irradiation. Secondly, the configurations are often not the same as the Spherical Code (i.e. points as spread out as possible), and in some cases it is beneficial to allow different sources to have different intensities.

The stability of the arrangements with respect to small imperfections was investigated, and it was found that standard deviations in angle of 0.035 rad and in intensity of 2% could lead to expected nonuniformities several times larger than the absolute minima. We then modified the formalism to account for the changing radius of the capsule, by using (scaled) time averaged expansion coefficients. The behaviour of the optimum configurations is qualitatively the same as in the stationary case, but the relevant values of d/a are different.

Further investigations will study whether having individual point sources at different distances to each other is beneficial. Whilst the expressions with which one must work are slightly messier, it will still be fairly straightforward to implement basin-hopping for this case. Early on in the investigations a genetic algorithm was developed to seek for new configurations. This worked, but was not as fast nor effective as the basin-hopping. However, it would allow the use of different cost functions, which would allow stability to imperfections to be taken into account. Finally, a deeper understanding of

the configurations that have been found is required, which will help find the exact minimum nonuniformity. We also note that the methods discussed in this paper can be straightforwardly applied to optimise arrangements for laser-driven systems for a given set of beam parameters and number of lasers.

9. Acknowledgments

We would like to thank Ian Cooper, whose initial project started this work. We also thank members of the Plasma Physics Group at Imperial College London for insightful discussions, and Robbie Scott for useful comments on the initial draft. We are grateful to the Imperial College Undergraduate Research Opportunities Programme for its financial support. Lastly, we thank the reviewer for their helpful comments.

References

[1] J. Nuckolls, et al., Laser compression of matter to super-high densities: Thermonuclear (ctr) applications, Nature 239 (1972) 139–142.

[2] National ignition facility experiment puts researchers at threshold of fusion ignition, https://www.llnl.gov/news/national-ignition-facility-experiment-puts-researchers-threshold-fusion-ignition, accessed: 2021-01-10.

[3] M. Murakami, D. Nishi, Optimization of laser illumination configuration for directly driven inertial confinement fusion, Matter and Radiation at Extremes 2 (2) (2017) 55–68. doi:10.1016/j.mre.2016.12.002.
URL https://doi.org/10.1016/j.mre.2016.12.002

[4] C. Lewis, J. McGlinchey, Quasi-monochromatic, projection radiography of dense laser driven spherical targets, Optics Communications 53 (3) (1985) 179–186. doi:10.1016/0030-4018(85)90327-x.
URL https://doi.org/10.1016/0030-4018(85)90327-x

[5] L. J. Perkins, R. Betti, K. N. LaFortune, W. H. Williams, Shock ignition: A new approach to high gain inertial confinement fusion on the national ignition facility, Physical Review Letters 103 (4) (Jul. 2009). doi:10.1103/physrevlett.103.045004.
URL https://doi.org/10.1103/physrevlett.103.045004

[6] W. Trickey, J. Pasley, Producing shock-ignition-like pressures by indirect drive, Plasma Physics and Controlled Fusion 61 (10) (2019) 105010. doi:10.1088/1361-6587/ab3007.
URL https://doi.org/10.1088/1361-6587/ab3007

[7] W. Trickey, J. Owen, C. Ridgers, J. Pasley, Controlling x-ray flux in hohlraums using burnthrough barriers, Physics of Plasmas 27 (10) (2020) 103301. doi:10.1063/5.0014798.
URL https://doi.org/10.1063/5.0014798

[8] Spherical code, https://mathworld.wolfram.com/SphericalCode.html, accessed: 2021-01-10.

[9] S. Skupsky, K. Lee, Uniformity of energy deposition for laser driven fusion, Journal of Applied Physics 54 (7) (1983) 3662–3671. doi:10.1063/1.332599.
URL https://doi.org/10.1063/1.332599

[10] P. W. Hatfield, S. J. Rose, R. H. H. Scott, The blind implosion-maker: Automated inertial confinement fusion experiment design, Physics of Plasmas 26 (6) (2019) 062706. doi:10.1063/1.5091985.
URL https://doi.org/10.1063/1.5091985

[11] D. J. Wales, J. P. K. Doye, Global optimization by basin-hopping and the lowest energy structures of lennard-jones clusters containing up to 110 atoms, The Journal of Physical Chemistry A 101 (28) (1997) 5111–5116. doi:10.1021/jp970984n.
URL https://doi.org/10.1021/jp970984n

[12] S. Kirkpatrick, C. D. Gelatt, M. P. Vecchi, Optimization by simulated annealing, Science 220 (4598) (1983) 671–680. doi:10.1126/science.220.4598.671.
URL https://doi.org/10.1126/science.220.4598.671

[13] R. Horst, P. M. Pardalos, N. V. Thoai, Introduction to Global Optimization - Nonconvex Optimization and Its Applications, Kluwer Academic Publishers, 2000.

[14] P. W. Hatfield, J. A. Gaffney, G. J. Anderson, S. Ali, L. Antonelli, S. B. du Pree, J. Citrin, M. Fajardo, P. Knapp, B. Kettle, B. Kustowski, M. J.

MacDonald, D. Mariscal, M. E. Martin, T. Nagayama, C. A. J. Palmer, J. L. Peterson, S. Rose, J. J. Ruby, C. Shneider, M. J. V. Streeter, W. Trickey, B. Williams, The data-driven future of high-energy-density physics, Nature 593 (7859) (2021) 351–361. doi:10.1038/s41586-021-03382-w.
URL https://doi.org/10.1038/s41586-021-03382-w

[15] P. Virtanen, R. Gommers, T. E. Oliphant, M. Haberland, T. Reddy, D. Cournapeau, E. Burovski, P. Peterson, W. Weckesser, J. Bright, S. J. van der Walt, M. Brett, J. Wilson, K. J. Millman, N. Mayorov, A. R. J. Nelson, E. Jones, R. Kern, E. Larson, C. J. Carey, İ. Polat, Y. Feng, E. W. Moore, J. VanderPlas, D. Laxalde, J. Perktold, R. Cimrman, I. Henriksen, E. A. Quintero, C. R. Harris, A. M. Archibald, A. H. Ribeiro, F. Pedregosa, P. van Mulbregt, SciPy 1.0 Contributors, SciPy 1.0: Fundamental Algorithms for Scientific Computing in Python, Nature Methods 17 (2020) 261–272. doi:10.1038/s41592-019-0686-2.

[16] R. H. Byrd, P. Lu, J. Nocedal, C. Zhu, A limited memory algorithm for bound constrained optimization, SIAM Journal on Scientific Computing 16 (5) (1995) 1190–1208. doi:10.1137/0916069.
URL https://doi.org/10.1137/0916069

[17] M. Murakami, K. Nishihara, H. Azechi, Irradiation nonuniformity due to imperfections of laser beams, Journal of Applied Physics 74 (2) (1993) 802–808. doi:10.1063/1.354869.
URL https://doi.org/10.1063/1.354869

[18] S. Atzeni, J. Meyer-ter Vehn, The Physics of Inertial Fusion: Beam Plasma Interaction, Hydrodynamics, Hot Dense Matter, Clarendon Press, Oxford, 2004. doi:10.1103/physrevlett.103.045004.